Scalable, printable, surfactant-free graphene ink directly from graphite

2013 Nanotechnology 24 205304

(http://iopscience.iop.org/0957-4484/24/20/205304)

Nanotechnology **24** (2013) 205304 (7pp) doi:10.1088/0957-4484/24/20/205304

Scalable, printable, surfactant-free graphene ink directly from graphite

X Han, Y Chen, H Zhu, C Preston, J Wan, Z Fang and L Hu

Department of Materials Science and Engineering, University of Maryland, College Park, MD 20742, USA

E-mail: binghu@umd.edu

Received 26 January 2013, in final form 8 March 2013
Published 23 April 2013
Online at stacks.iop.org/Nano/24/205304

Abstract
In this manuscript, we develop printable graphene ink through a solvent-exchange method. Printable graphene ink in ethanol and water free of any surfactant is dependent on matching the surface tension of the cross-solvent with the graphene surface energy. Percolative transport behavior is observed for films made of this printable ink. Optical conductivity is then calculated based on sheet resistance, optical transmittance, and thickness. Upon analyzing the ratio of dc/optical conductivity versus flake size/layer number, we report that our dc/optical conductivity is among the highest of films based on direct deposited graphene ink. This is the first demonstration of scalable, printable, surfactant-free graphene ink derived directly from graphite.

(Some figures may appear in colour only in the online journal)

1. Introduction

Graphene is a versatile material and has spurred enormous interests in research dedicated to transparent electrodes [1–5], high-speed transistors [6] and energy storages [7–12]. A single layer of graphene without defects possesses an optical transmittance of 97.7% and a sheet resistance of $\sim$100 Ω sq^{-1} [1, 13, 14]. A random network of graphene flakes is promising for transparent conductor applications due to its low percolation threshold and high DC conductivity. Solution based graphene films also have a much lower cost. Recent works on solution processed graphene films report compelling results [8, 15–17]; however, the processes involve the use of toxic solvents, high-temperature thermal reduction from graphene oxide, or non-scalable film fabrication methods. Scalable graphene ink with nontoxic solvents is needed. A typical graphene solution is based on solvents with high boiling points, e.g. *N*-methylpyrrolidone (NMP) that needs a long drying time [18]. Aqueous dispersion is preferred [19], but typically it has a high surface energy that does not allow a good wetting or drying. Wetting agents and surfactants, such as fluorosurfactant, sodium dodecylbenzenesulfonate (SDBS), and Triton X100, are needed to lower the surface energy of dispersion for coating purposes [20, 21], but wetting agents and surfactants are insulating and decrease the film conductivity. For certain applications such as batteries, these agents may also cause side reactions and need to be removed after film fabrication. By virtue of a posted-treatment using a strong acid, excellent optoelectronic properties were obtained for single-walled carbon nanotubes (SWNT) on glass substrate [22]. Surfactant-free graphene ink with a low surface energy and a low boiling point that enables roll-to-roll printing is still needed.

Based on the principle that the surface energy of graphene and the surface tension of dispersion solvent need to balance, here we applied a cross-solvent to achieve printable and stable graphene ink via solvent exchange. We used a polydimethylsiloxane (PDMS)-transfer method to investigate the fundamental optoelectronic properties. Optical conductivity (opt) is calculated for films with obtained sheet resistances and optical transmittances. Usually, either the value of dc/opt conductivity ratio or T^{10}/R_s (T: transmittance, R_s: sheet resistance) can be used as a figure of merit (FOM) to evaluate transparent conductive film properties [23, 24]. For convenient comparison of our printing graphene films with the values reported in literature, the dc/opt conductivity ratio is employed as FOM in this work. The dc/opt conductivity ratio clearly shows a strong dependence on the graphene flake size. Scalable ink was demonstrated and applied on a flexible plastic substrate to fabricate a transparent and conductive film.

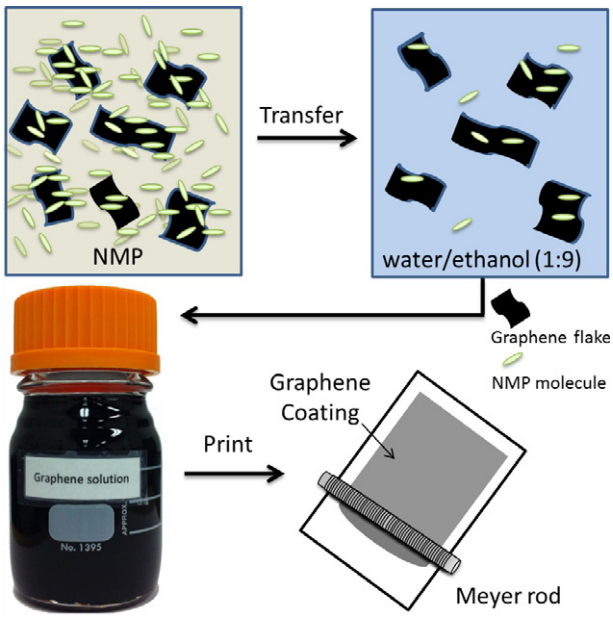

Figure 1. Schematic for printable graphene ink based on a solvent-exchange approach with a cross-solvent. Graphite is exfoliated and dispersed in NMP with the help of sonication, then transferred in a water/ethanol mixed solvent by filtration and re-dispersion. Surfactant-free graphene ink derived directly from graphite can be coated on substrates with scalable methods followed by infrared drying.

Dispersed graphene flakes in solution were obtained from solution-phase exfoliation of graphite via sonication in NMP, and then transferred into a cross-solvent of water/ethanol (1:9, volume ratio) through filtration and re-dispersion. Note that we do not use any surfactants for the transfer here, which is favorable for many applications. Due to the quick evaporation of the cross-solvent, the resulting dark solution is easily coated on substrates (PET and glass) using a Meyer rod. A few minutes of infrared light irradiation facilitates the formation of a uniform film. Infrared light irradiation is used to create a temperature gradient that can drive a drying pattern toward a uniform film formation [25]. Figure 1 schematically illustrates the process for coating and drying. Nanomanufacturing with roll-to-roll printing is an important step for practical applications of devices that integrated graphene films. Prior studies demonstrate the dispersions of graphene (not graphene oxide) in organic solvents such as NMP and DMF. Continuous graphene printing, however, is not yet demonstrated with benign solvents.

2. Experimental section

2.1. Materials

Graphite flakes, anhydrous 1-methyl-2-pyrrolidinone (NMP) and ethanol (proof 200) were purchased from Sigma-Aldrich. Deionized water was used to prepare the cross-solvent of water and ethanol.

2.2. Preparation of graphene solution in NMP

The preparation of graphene follows the literature with a slight modification: liquid-phase exfoliation of graphite [26]. Typically, 200 ml of NMP and 0.66 g graphite is mixed in 250 ml flask and then sonicated in a bath sonicator for 90 h. After standing overnight, the upper 150 ml solution is taken out and kept for future transfer.

2.3. Transfer of graphene from NMP to water/ethanol cross-solvent for printable ink

20 ml of the prepared graphene solution in NMP is first vacuum-filtrated using a PTFE filter with a pore size of 0.45 μm, and then the resulting solid is put in a 50 ml centrifuge tube containing 20 ml of water/ethanol (1:9, volume ratio). After a few minutes of vortex and sonication, the graphene can be re-dispersed into the water/ethanol cross-solvent completely and the filter is ready to remove. The process is performed three times to get the printable graphene ink.

2.4. Fabrication of film and sheet resistance (R_s) and transmittance tests

The film fabrication is done by Meyer rod coating. Normally 100 μl of the above graphene ink is dropped on the part of substrates of PET or glass, following drawing using Meyer rod (rod #18). To promote the film conductivity, the coating is carried on several times. The sheet resistance (R_s) is measured using the surface resistivity meter (RC2175, EDTM, Inc.). The transmittance is recorded with a Lambda 35 UV/Vis spectrophotometer that uses an integrated sphere (PerkinElmer).

2.5. TEM and SEM tests

Due to the quick evaporation of the cross-solvent, the TEM sample is directly prepared by dropping 20 μl of the graphene ink on a TEM grid. For SEM, the graphene film is observed on an AAO filter by vacuum filtration, and also directly on PET or glass after rod coating. To enable the samples conductivity, carbon tape is used to connect the graphene sample's top surface with SEM sample stages. TEM is performed on a JEOL JEM 2100 with an electron gun of LaB6, and SEM images are on a Hitachi SU-70.

3. Results and discussion

We first investigated the lateral size, thickness, and the quality of the graphene flakes in the dispersion, which govern the transport and optoelectronic properties of graphene films. A selective area electron diffraction (SAED) pattern of transmission electron microscopy (TEM) in figure 2(a) indicates a few-layer graphene in the graphene flakes. To preserve their dimensions, graphene flakes on anodic aluminum oxide (AAO) filters with a fast filtration process were made to avoid the agglomeration during the drying process. As shown in figure 2(b), the graphene flakes on the AAO filter are transparent to electrons during the scanning electron microscopy (SEM) test and the AAO filter underneath can be observed clearly, which indicates

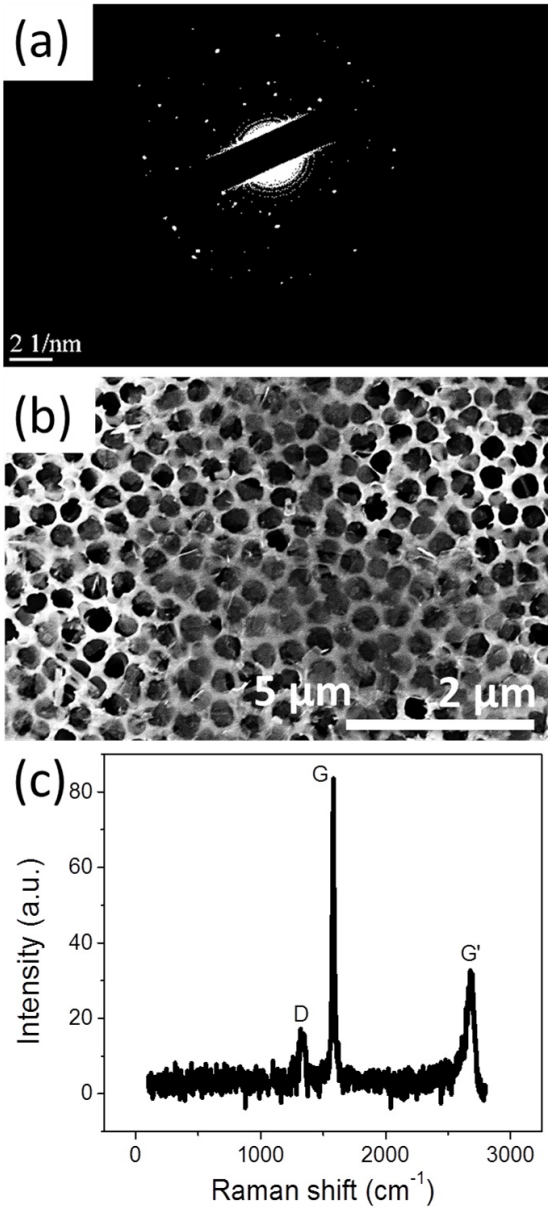

Figure 2. (a) A TEM diffraction pattern of the graphene flakes. (b) A SEM image of graphene flakes on an AAO filter. The average size of graphene flakes is ∼1 μm. (c) Raman spectroscopy for a free-standing graphene film. The low I_D/I_G ratio indicates the high quality of the graphene flakes.

the graphene flakes are thin. It is estimated from the SEM images that the average lateral size is 1 μm, which is defined as the maximum length of the graphene flakes. The average thickness measured is about 4.5 nm by using an atomic force microscopy (AFM, not shown). Given that individual graphene monolayers appear to be ∼1 nm thick with AFM [27], the layer number for the graphene flakes in our dispersion is ∼4–5. Raman spectroscopy is used to characterize the quality of the graphene flakes [28]. As shown in figure 2(c), the Raman spectrum for the graphene flakes has two distinct peaks located at ∼1580 cm^{-1} (G) and ∼2680 cm^{-1} (G′). The D-peak at ∼1320 cm^{-1} is due to the sp^3 hybridization. The intensity ratio of the D-peak and G-peak is widely used to quantify the quality of graphene. Figure 2(c) displays our graphene samples have a high intensity of G-peak, a sharp G′, and low I_D/I_G ratio (0.15), which clearly indicate the high quality of graphene flakes with a small thickness and little amount of defects in the dispersion [29]. The weak D-peak mainly results from the edge effect [26].

To explore the optoelectronic properties of the graphene flakes, graphene stacked films were made using different volumes (from 100 to 1000 μl) of ink by a vacuum filtration, followed by PDMS transfer printing. This method has several advantages for studying the optoelectronics properties of flakes: (1) it preserves the dimension of flakes due to the fast deposition; (2) it allows the precise control of the film thickness and sheet resistance; (3) it allows the measurement of a film's optical properties because of the transparency of PMDS. Figure 3(a) shows a graphene film on a transparent PDMS stamp, which is transferred from graphene film filtrated on an AAO filter by vacuum filtration. This method has been used for evaluating the performance of other transparent conductors [30]. A FOM can be obtained by measuring the optical transmittance and sheet resistance. The FOM in this study is defined as σ_{dc}/σ_{opt}, where σ_{dc} and σ_{opt} are dc and optical conductivity, separately. Optical transmittance and sheet resistance can be described with equation (1):

$$T = \left(1 + \frac{1}{2R_s}\sqrt{\frac{\mu_0}{\varepsilon_0}}\frac{\sigma_{opt}}{\sigma_{dc}}\right)^{-2} = \left(1 + \frac{188\ (\Omega)}{R_s}\frac{\sigma_{opt}}{\sigma_{dc}}\right)^{-2} \quad (1)$$

where T is the optical transmittance and R_s is the sheet resistance. Sheet resistance and optical transmittance in the visible and near infrared range are presented in figures 3(c) and (d) for films made of different ink volumes. The concentration of the graphene ink is 0.43 mg ml^{-1}. As the volume increases from 100 to 1000 μl, the optical transmittance at 550 nm decreases from 82% to 7%. The sheet resistance changes from an insurmountable quantity to 1000 Ω sq^{-1}. A two-dimensional percolation behavior of randomly distributed conductive objectives is expected, which predicts that the conductance versus surface coverage of conductive objects follows equation (2) [31]:

$$G \sim (A - A_0)^{\alpha} \quad (2)$$

where $G = 1/R_s$ is the sheet conductance, A is the surface coverage, A_0 is the critical surface coverage to form a percolative conductive path, and α is a constant for the power law. α equals 4/3 for a 2D system, and 2 for a 3D system [23]. Surface coverage of the graphene network is proportional to the amount of dispersion used for the film fabrication; therefore we can re-write the percolation equation (2) as

$$G = G_0(V - V_0)^{\alpha} \quad (3)$$

where V is the volume of dispersion, V_0 is the critical volume to form a percolative conductive path, and G_0 the percolative conductance. We fit our data using equation (3), as shown in figure 3(d). The measured data fits well with the 2D percolation model, with $G_0 = 4.95 \times 10^{-8}$ S, $V_0 = 170$ μl, and $\alpha = 1.46$.

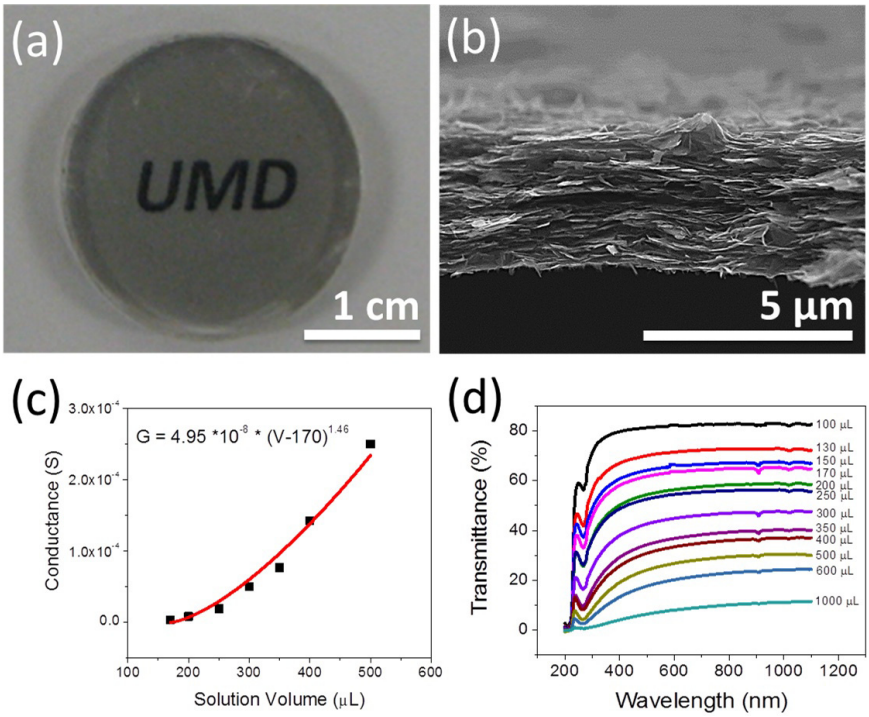

Figure 3. (a) A transparent and conductive graphene film transferred onto a PDMS stamp. The University of Maryland (UMD) logo under the graphene-PDMS film is clearly visible, which illustrates the optical transparency of the transferred film. Note that the PDMS stamp is with a smaller area than the AAO filter. (b) The cross-section of graphene showing that the flakes are interconnected to form a 2D conductive network. (c) Conductance versus the graphene ink volume with a percolation behavior. The data fits well with the 2D percolation model. (d) The optical transmittance of graphene films with a tunable range on a PDMS stamp, where the transmittance of PMDS was excluded.

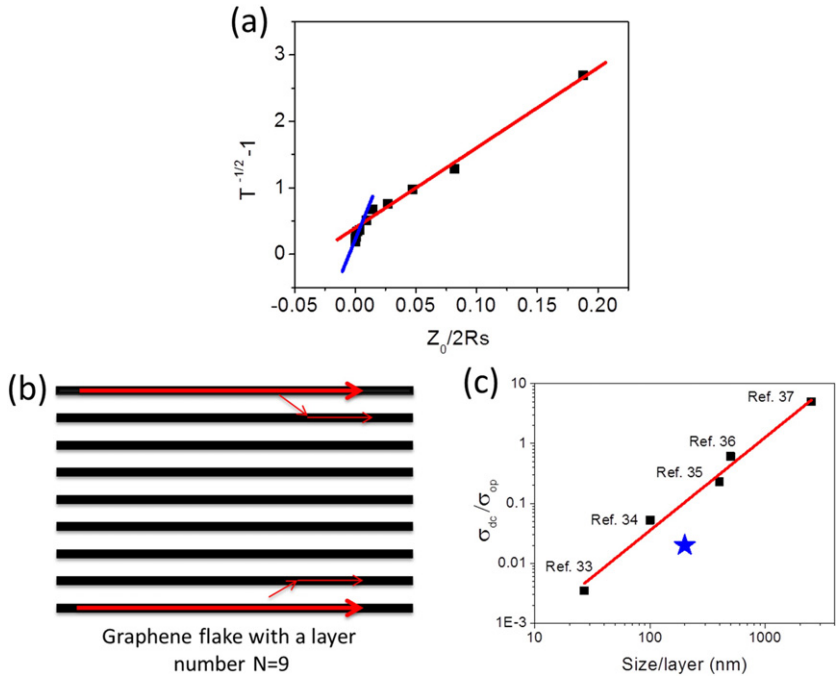

Figure 4. (a) $T^{-1/2} - 1$ versus $Z_0/2R_s$ based on an optical transmittance at 550 nm and sheet resistance with $Z_0 = 376$ for graphene. The two slopes (σ_{op}/σ_{dc}) indicate a 2D to 3D transition in graphene films as the thickness increases. (b) A schematic to illustrate the coupling of current flow on a single sheet of multi-layer graphene. (c) The FOM (σ_{dc}/σ_{op}) versus size/layer number for graphene films. As the aspect ratio increases, the FOM increases. The FOMs for graphene films fabricated with other methods are calculated from previous data given in the literature [33–37].

We further investigate the optoelectronic properties of graphene films on PDMS in order to understand the quality of the flakes based on FOM of the transparent films. Data of the conductance and optical transmittance at 550 nm from figures 3(c) and (d) for films based on different dispersion volumes is plotted in figure 4(a). From equation (1), the slope

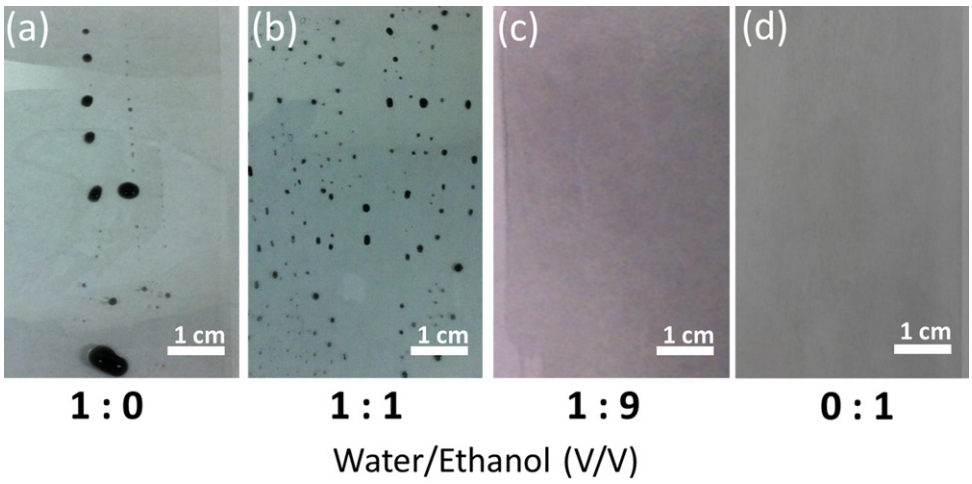

Figure 5. A Meyer rod coating of graphene ink with different water/ethanol ratio. As ethanol fraction increases, the surface tension decreases, which leads to an improved coating.

of $T^{-1/2} - 1$ versus $188/R_s$ is 1/FOM. The data in figure 4(a) clearly indicates that there are two regions with different FOMs. The FOM is 0.02 for a thin film and 0.083 for a thick film. The transition from thin to thick region corresponds to a transition of 2D to 3D, which is observed in carbon nanotube and graphene networks [32]. This transition is due to the interlayer coupling of the graphene flakes. The thickness of graphene flakes in our dispersion is ∼4.5 nm, corresponding to a layer number of ∼5. It is important to obtain a large aspect ratio, the lateral size versus the layer number in order to achieve a smaller percolation threshold. The layer number is also critical since the current will require a certain distance to couple into the inner layers. As shown in figure 4(b), current will start from the outer layers at junctions and couple into the inner layers. For dense networks, the layer–layer distance is less than the coupling distance. The current, therefore, will mainly flow along the outer layers. The inner layers will not contribute much to the electrical conductance, but instead absorb or reflect the light.

We have evaluated the FOM, σ_{dc}/σ_{op}, for transparent graphene films made of different methods. The sheet resistance, optical transmittance, lateral size, and the layer number were obtained from literature [33–37]. There is a clear trend that the FOM increases as the size/layer number ratio increases (the dashed line is for clarity of the trend). There are many other factors that affect the performance of the films, such as the graphene–graphene contact and the defects on graphene flakes. The most important parameter for achieving transparent graphene films with a high FOM is the aspect ratio. Chemical vapor deposition (CVD) creates a graphene film size of up to a centimeter. Reduced graphene oxide typically leads to a size of 1–20 μm [35, 38, 39]. Graphene from direct dispersion typically has a much smaller aspect ratio and leads to a much smaller FOM. Graphene derived directly from graphite is important for many applications, especially when cost and post-process compatibility are important. For example, most reduction methods for graphene oxide are not compatible with plastic substrates. For energy storage devices, the reduction step cannot be applied for the electrode composites. The FOM of our graphene film, 0.08, is comparable with the values based on other non-printable solvents [33].

The above analysis shows that our graphene dispersion consists of flakes with excellent properties, which is comparable to the best values reported in literature. Opposed to previous directly exfoliated graphene inks reported in the literature [33, 36], our graphene dispersion based on water and ethanol mixed solvent is printable. Also, the as-obtained graphene ink was rather stable for at least half a year, especially when the graphene concentration was less than 0.5 mg ml^{-1}. Graphene ink with a higher concentration was not as stable and some precipitate formed in the bottom of the container after a few days. After the precipitation, the color of the top portion of the solution is still dark (graphene flakes dispersion) and stable for several months. We speculate that the stabilization is related to the effect of cross-solvent and possibly a trace amount of NMP residual. Water has a high surface tension (72.8 dynes cm^{-1} at 20 °C) and ethanol has a low value (22.3 dynes cm^{-1} at 20 °C). The surface tension of the mixture with water and ethanol is likely to match closely the surface free energy of graphene (46 mJ m^{-2}) and natural graphite (54.8 mJ m^{-2}) at room temperature [40]. Not only graphene can disperse but also graphite can be exfoliated in the cross-solvent. We tested the exfoliation effect of the cross-solvents with various ratios of ethanol and water. The results confirm that the cross-solvents lead to exfoliation and can disperse graphite (not shown here). When transferring graphene from NMP to the cross-solvent for printing purposes, the water to ethanol volume ratio needs to be optimized. Both the wetting and drying dynamics are critical for achieving a uniform graphene film on a substrate. We carried out coating experiments on mixed solvents with various water/ethanol ratios. As the ethanol amount increases from 1:0 to 1:1 (water/ethanol), the wetting of graphene ink on a plastic PET substrate improves dramatically, however the ethanol evaporates much faster than water, many droplets were formed during the drying (figures 5(a) and (b)), and finally coffin rings left. When the ethanol amount increased

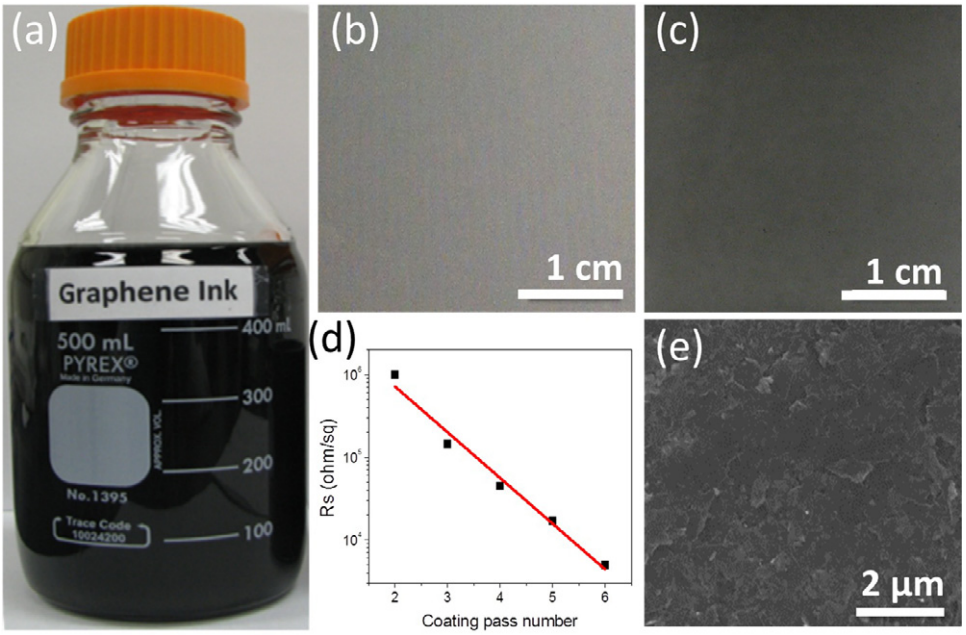

Figure 6. (a) A picture of scalable and printable graphene ink with a volume of 500 ml transferred from NMP solution. The transfer yield is nearly 100%. Uniform graphene coating on plastic (b) and glass (c) substrates with a size of 3 cm × 3 cm, respectively. (d) Sheet resistance versus coating pass number on polyethylene terephthalate (PET) substrate. (e) SEM image of printed graphene flakes in (b).

up to 1:9 (water/ethanol), both the wetting and drying were uniform (figure 5(c)). When transferring to pure ethanol, the graphene ink can be still coated and dried on PET substrate uniformly (figure 5(d)). However the dispersion of graphene in pure ethanol is non-stable, and graphene flake aggregation is formed in a few hours. Thus the presence of a small amount of water in the solution (forming co-solvent) is important for the solution stability. The ratio of water to ethanol needs to be optimized to achieve good stability and good coating capability. This is the first demonstration of continuous printable ink that is based on a benign solvent with a low surface energy. No surfactant is used, which avoids the post-processing usually necessary for the film treatment.

After transferring from a NMP solution to water/ethanol (1:9, v/v), the graphene ink shown in figure 6(a) is fully printable, which enables large-scale nanomanufacturing. The transfer yield is nearly 100%. Meyer rod coating allows us to control the wet thickness precisely, which is widely used in industry for large-scale manufacturing [41]. The process is easily scaled to industrial levels with the low-cost solvent and raw graphite material. We applied the graphene ink on flexible plastic (figure 6(b)) and normal glass (figure 6(c)) to demonstrate a scalable printing on different substrates.

To evaluate the film resistance versus coating pass number, the functional relationship is recorded in figure 6(d) that the logarithmic sheet resistance (R_S) is in direct proportion to the pass number (coating repetition times). The SEM image in figure 6(e) displays the films with pass number 6 are highly uniform. The Meyer rod number is 18, which forms a wet thickness of 45.7 μm for each individual coating pass. The sheet resistance decreases dramatically as the coating number increases. Typically, the concentration for the graphene ink is 0.43 mg ml^{-1}. Optical transmittances of 40% are achieved with directly printed films on a plastic substrate by multiple rod-coating steps. The transmittance is more than 90% with a much higher resistance for a single coating. Adhesion of film on a substrate is critical for film handling and device applications with a good stability. Since no binders are used in the dispersion, the obtained graphene film has a delamination problem. This delamination problem can be solved by a surface coating with a thin layer of conductive binder, which has been widely used for SWNT films [42]. A similar polymer coating can be applied on our graphene films. Our graphene ink has a very low viscosity close to water due to its graphene concentration. The patterning resolution with such inks will not only depend on the substrate choice, but also on the printing and drying processes. We expect a ~10 μm resolution is readily available with an ink jet printing method, similar to printed SWNT films with inks of a low viscosity [13]. For flexible electronics applications, a few tests are important, including the resistance change over bending with a different radius and the performance under different external loading conditions. Flexibility and stretchability of graphene films on substrates have been demonstrated before [43–45]. SEM images examine the surface morphology of the graphene flakes coated on plastic substrate (figure 6(e)). The performance of the transparent electrode directly coated with the printable ink enables anti-static coating [32]. Further improvement mostly relies on increasing the aspect ratio for graphene flakes in the dispersion, which may be achieved by optimizing the sonication process, the choice of solvent, and some other new methods for fabricating large-area graphene flakes without cutting the lateral dimensions.

4. Conclusion

We successfully demonstrate printable and surfactant-free graphene ink with a solvent-exchange method to switch from NMP to a water/ethanol cross-solvent. A percolation behavior was observed in the random network of graphene flakes. Sheet resistance and optical transmittance data adhere to a printed graphene film, with two distinct op/dc regions corresponding to a transition from 2D to 3D. We also demonstrate scalable rod coating on plastic and glass substrates, which enables roll-to-roll coating and thus promotes large scalability. The graphene size needs to increase to form a lower percolation threshold and achieve a higher performance. The surfactant-free graphene ink in a water/ethanol mixed solvent is applicable to flexible electronics, energy storage devices, and biological devices.

Acknowledgments

L Hu acknowledges the financial startup support from University of Maryland. We acknowledge the support of the Maryland NanoCenter and its NispLab and SAC. The NispLab is supported in part by the NSF as a MRSEC shared experimental facility.

References

[1] Bae S *et al* 2010 *Nature Nanotechnol.* **5** 574–8
[2] Kim K S, Zhao Y, Jang H, Lee S Y, Kim J M, Kim K S, Ahn J-H, Kim P, Choi J-Y and Hong B H 2009 *Nature* **457** 706–10
[3] Li X, Zhu Y, Cai W, Borysiak M, Han B, Chen D, Piner R D, Colombo L and Ruoff R S 2009 *Nano Lett.* **9** 4359–63
[4] Wang X, Zhi L and Muellen K 2008 *Nano Lett.* **8** 323–7
[5] Wu J, Agrawal M, Becerril H A, Bao Z, Liu Z, Chen Y and Peumans P 2010 *ACS Nano* **4** 43–8
[6] Liao L, Lin Y C, Bao M Q, Cheng R, Bai J W, Liu Y A, Qu Y Q, Wang K L, Huang Y and Duan X F 2010 *Nature* **467** 305–8
[7] Geim A K 2009 *Science* **324** 1530–4
[8] Allen M J, Tung V C and Kaner R B 2010 *Chem. Rev.* **110** 132–45
[9] Avouris P, Chen Z and Perebeinos V 2007 *Nature Nanotechnol.* **2** 605–15
[10] Brownson D A C, Kampouris D K and Banks C E 2011 *J. Power Sources* **196** 4873–85
[11] Hou J, Shao Y, Ellis M W, Moore R B and Yi B 2011 *Phys. Chem. Chem. Phys.* **13** 15384–402
[12] Pumera M 2009 *Chem. Rec.* **9** 211–23
[13] Hecht D S, Hu L and Irvin G 2011 *Adv. Mater.* **23** 1482–513
[14] Nair R R, Blake P, Grigorenko A N, Novoselov K S, Booth T J, Stauber T, Peres N M R and Geim A K 2008 *Science* **320** 1308–8
[15] Wang S, Ang P K, Wang Z, Tang A L L, Thong J T L and Loh K P 2010 *Nano Lett.* **10** 92–8
[16] Tung V C, Chen L-M, Allen M J, Wassei J K, Nelson K, Kaner R B and Yang Y 2009 *Nano Lett.* **9** 1949–55
[17] Wang J, Liang M, Fang Y, Qiu T, Zhang J and Zhi L 2012 *Adv. Mater.* **24** 2874–8
[18] Khan U, O'Neill A, Lotya M, De S and Coleman J N 2010 *Small* **6** 864–71
[19] Li D, Muller M B, Gilje S, Kaner R B and Wallace G G 2008 *Nature Nanotechnol.* **3** 101–5
[20] Walters K B, Schwark D W and Hirt D E 2003 *Langmuir* **19** 5851–60
[21] Dan B, Irvin G C and Pasquali M 2009 *ACS Nano* **3** 835–43
[22] Li X, Gittleson F, Carmo M, Sekol R C and Taylor A D 2012 *ACS Nano* **6** 1347–56
[23] Hu L, Hecht D S and Gruener G 2010 *Chem. Rev.* **110** 5790–844
[24] Li J, Hu L, Liu J, Wang L, Marks T J and Gruener G 2008 *Appl. Phys. Lett.* **93** 083306
[25] Hu L, Gruner G, Jenkins J and Kim C J 2009 *J. Mater. Chem.* **19** 5845–9
[26] Hernandez Y *et al* 2008 *Nature Nanotechnol.* **3** 563–8
[27] Novoselov K S, Geim A K, Morozov S V, Jiang D, Zhang Y, Dubonos S V, Grigorieva I V and Firsov A A 2004 *Science* **306** 666–9
[28] Zhu Y, Murali S, Cai W, Li X, Suk J W, Potts J R and Ruoff R S 2010 *Adv. Mater.* **22** 3906–24
[29] Ferrari A C *et al* 2006 *Phys. Rev. Lett.* **97** 187401
[30] Zhou Y X, Hu L B and Gruner G 2006 *Appl. Phys. Lett.* **88** 123109
[31] Pike G E and Seager C H 1974 *Phys. Rev.* B **10** 1421–34
[32] Kaempgen M, Duesberg G S and Roth S 2005 *Appl. Surf. Sci.* **252** 425–9
[33] Chang H, Wang G, Yang A, Tao X, Liu X, Shen Y and Zheng Z 2010 *Adv. Funct. Mater.* **20** 2893–902
[34] Liu Y, Gao L, Sun J, Wang Y and Zhang J 2009 *Nanotechnology* **20** 465605
[35] Geng J, Liu L, Yang S B, Youn S-C, Kim D W, Lee J-S, Choi J-K and Jung H-T 2010 *J. Phys. Chem.* C **114** 14433–40
[36] Green A A and Hersam M C 2009 *Nano Lett.* **9** 4031–6
[37] Reina A, Jia X, Ho J, Nezich D, Son H, Bulovic V, Dresselhaus M S and Kong J 2008 *Nano Lett.* **9** 30–5
[38] Zhao J, Pei S, Ren W, Gao L and Cheng H-M 2010 *ACS Nano* **4** 5245–52
[39] Yin Z, Sun S, Salim T, Wu S, Huang X, He Q, Lam Y M and Zhang H 2010 *ACS Nano* **4** 5263–8
[40] Wang S, Zhang Y, Abidi N and Cabrales L 2009 *Langmuir* **25** 11078–81
[41] Stahl H, Appenzeller J, Martel R, Avouris P and Lengeler B 2000 *Phys. Rev. Lett.* **85** 5186–9
[42] Ou E C W *et al* 2009 *ACS Nano* **3** 2258–64
[43] Kim K S, Zhao Y, Jang H, Lee S Y, Kim J M, Kim K S, Ahn J H, Kim P, Choi J Y and Hong B H 2009 *Nature* **457** 706–10
[44] Chen Z, Ren W, Gao L, Liu B, Pei S and Cheng H-M 2011 *Nature Mater.* **10** 424–8
[45] Yan C, Cho J H and Ahn J H 2012 *Nanoscale* **4** 4870–82